

MEASUREMENTS OF FOREST INVENTORY PARAMETERS ON TERRESTRIAL LASER SCANNING DATA USING DIGITAL GEOMETRY AND TOPOLOGY

István Pál

Lehrstuhl für Waldwachstumskunde
Technische Universität München
85354 Freising, Am Hochanger 13, Germany
Istvan.Pal@lrz.tum.de
<http://www.wwk.forst.wzw.tum.de/research/projects/interreg/>

KEY WORDS: digital geometry, digital topology, image processing, skeletonization, contrast enhancement, fractal dimension, LIDAR, terrestrial laser scanning

ABSTRACT:

This paper gives some mathematical methods for the automatic analysis and determination of forest management parameters in particular for the measurements of geometrical sizes on terrestrial scanning laser data using segmentation of the objects with iterative contrast enhancement, fractal dimension, skeletonization and local digital geometry and topology (LDGT).

1 INTRODUCTION

Terrestrial laser scanner (LIDAR) are used more and more in the forestry. The manual measurement of forest relevant parameters are very cost-intensive and time-consuming tasks, which can be supported with LIDAR data acquisition. By using 3D terrestrial laser scanning instruments the distances and other geometrical sizes in 3D-space can be measured on the digital data set. This data can be used for semi-automatic and/or automatic extraction of the forest relevant parameters. The geometrical primitives, structures and features of the tree crowns, tree stems such as stem position, height, length, diameter of the stem, size/volume of the leaf area etc. play a very important role in the forest management. An automatic or computer based extraction of these parameters is of great relevance for the forest inventory.

In this paper we will focus on the mathematical, numerical and digital-geometrical methods to extract forest relevant features on digital pictures (2D) and 3D data sets, in particular geometric measurement of the stem diameter at breast height (DBH). However we will focus mainly on the tree diameter calculation, because on the one-scan pictures the whole trees are mostly not available in all cases, but it is also possible to derive the other relevant inventory informations using the suggested methods. There will be used also common image processing algorithms for the picture analysis, as well as for the segmentation of the objects.

The aim of the paper is to develop mathematical founded algorithms for the supporting of the extraction of a subset of laser points, point clouds and regions from LIDAR data for the geometrical measurements and numerical calculations. But the statistical evaluation, a comparison the manual measurement with laser measurement will be here not discussed.

2 THE LIDAR DEVICE AND DATA

For the data acquisition the Riegl LMS-Z360 terrestrial laser scanner (see Fig. 1) was used. The Riegl scanner provides 2D, 3D data and true colour information (separate digital camera) about the 3D scene. The laser scanner measures the distance and the intensity to the nearest object point in a $[0..360]$ and $[-50..40]$ degree polar-system (see Fig. 2), which can be converted into an



Figure 1: The Riegl laser scanner in forest measurement in Freising, Germany

intensity 2D panorama picture, as well. For the automatic extraction and analysis of the forest management parameters will be used both the 2D intensity image and the 3D raw data set, but currently without the combination with the colour informations.

The data was recorded in the Bavarian forest - Böhm forest in

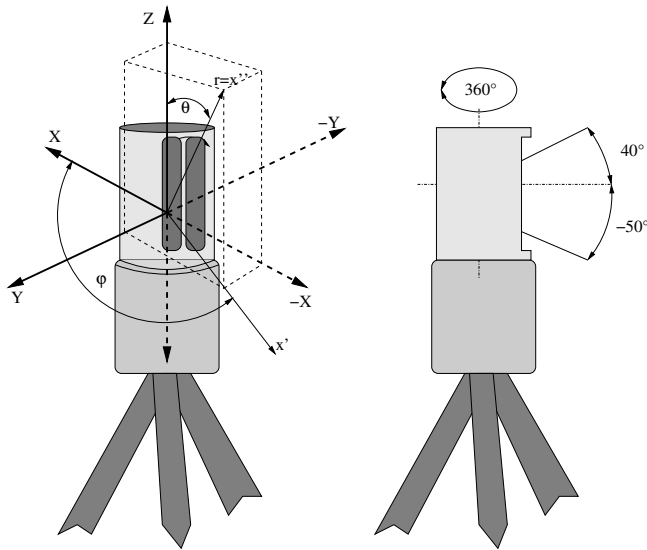


Figure 2: The horizontal and vertical scanning range of Riegl laser scanner.

German and Czech range. From an inventory point 3-5 measurements including the central point were made. In this work we will use only the data set from the central acquisition.

3 IMAGE PROCESSING OF THE LIDAR DATA

Our approach to the geometrical, real-size measurements on LIDAR data is based on the segmentation and skeletonization of the 2D panorama pictures and on the correction/extension of this information from the 3D data set. On the segmented pictures with the help of the skeletonized image and using local digital geometry and topology (LDGT) the forest relevant sizes e.g. the tree-trunk diameter can be determined and measured.

3.1 Image Filtering and Segmentation

For the image processing tasks the 2D panorama pictures (see Fig. 3 /a/) will be used. In the first step the panorama image is filtered with a Gaussian filter $G(x, y) = \exp(-\frac{x^2+y^2}{2\sigma^2})$ in order to remove and reduce the noisy artifacts. After that the image is binarized and segmented. The segmentation is based on an iterative contrast enhancement method (Pál and etal., 1996) which extracts the thin line-like (1-2 pixel wide) structures using a mask. The segmentation is taken by the following non-linear transformation:

$$b'_{ij} = \lambda \cdot b_{ij} \cdot \left(\frac{\max_l(r_l) - \min_l(r_l)}{\max_l(r_l) + \min_l(r_l)} \right)^\mu, \quad (1)$$

where b_{ij} is the reference pixel, $\lambda = 1.8$ and $\mu = 0.2$ are variable parameters but here empirical determined and r_l ($l \in [1..4]$) the direction sums over the reference pixel b_{ij} . The transformation is used iteratively k -times ($k = 3 \dots 6$) and in each step the size of the mask will be increased in which the r_l 's are determined, but always were used 4 directions. Parallel to this step a simple binarization of the original picture was done and added to the contrast enhanced image and to end the segmentation process a renewed binarization was carried out. The result is shown on the Fig. 3 (b). The characteristic of this segmentation method and comparison with another line segmentations and how it works on noisy images was shown in (Pál, 2002).

The result of this segmentation on an other, Faro LIDAR instrument is shown on the Fig. 4.

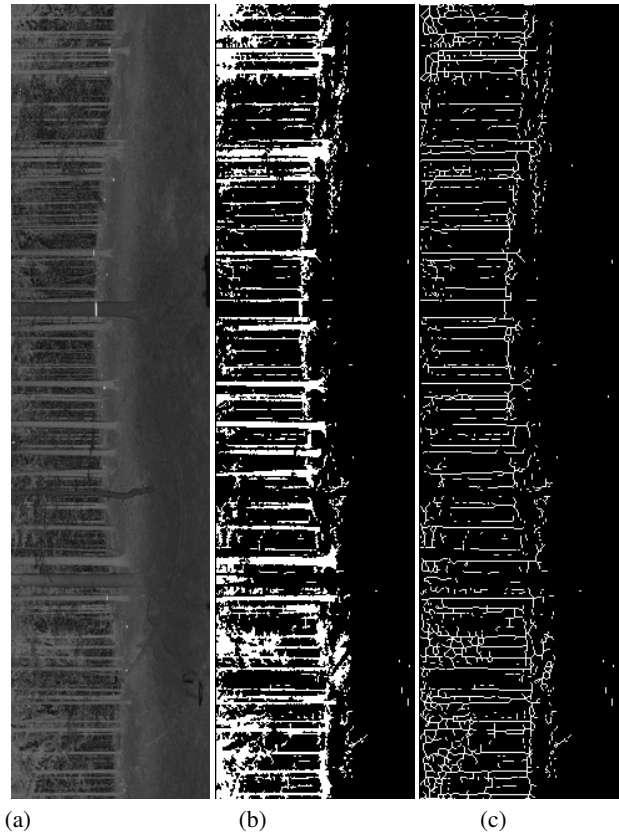


Figure 3: The pictures are 90 degree rotated. (a) Original polar picture by the Riegl scanner (size 750 × 3000 pixels), (b) segmented picture, (c) skeletonized picture



Figure 4: (top) Original picture by the Faro scanner, (bottom) the segmented picture,

3.2 Skeletonization

Skeletonization or thinning is used for the determination of the middle line of the segmented or binarized geometrical object on the digital picture. The skeleton picture can be used for measurements on the digital image, maybe for masking or together

with another pictures. So it can be used for the calculation of the length of the tree trunk, but also for the tree diameter calculation. There were studied and tested numerous skeletonization algorithms for 2D pictures described in (Riazanoff et al., 1990, Sirjani and Cross, 1991, Ge and Fitzpatrick, 1996, Dyer Charles and Rosenfeld, 1979, Bräunl et al., 1995, Pavlidis, 1990, Zamperoni, 1989, Klette and Zamperoni, 1995, Datta and Parui, 1994), but the best result was achieved by the Zhou suggested technique (Zhou et al., 1995). This algorithm was modified to become 1 pixel wide line structures as to reduce the (2×2) -structures on the digital picture.

3.3 The modified Algorithm by Zhou

The Zhou's algorithm is a sequential process to eliminate the boundary pixels which satisfy some topological conditions. The neighbour structures P_i and Q_i , the previous $PN(\cdot)$ and current neighbour $CN(\cdot)$, the connectivity function $T(\cdot)$ and the matching function $M(\cdot)$ are used such as in the Zhou's algorithm.

Definition 1. In the original and in the marked picture the symbols P_i and Q_i , $i \in \{0, 1, 2, \dots, 8\}$ represent the pixels with the following (3×3) -neighbour structure:

$$\begin{matrix} P_1 & P_2 & P_3 & Q_1 & Q_2 & Q_3 \\ P_8 & P_0 & P_4 & Q_8 & Q_0 & Q_4 \\ P_7 & P_6 & P_5 & Q_7 & Q_6 & Q_5 \end{matrix}, \quad (2)$$

where P_i and Q_i have the value 1 or 0 (object or background pixel) on the binary picture.

Definition 2. The previous neighbour of the pixel P_0 is defined as follows:

$$PN(P_0) = \sum_{i=1}^8 P_i, \quad (3)$$

Using $PN(P_0)$ can be decided about a pixel P_0 which is an object pixel in original image, whether this pixel is a boundary pixel or not.

Definition 3. The current neighbour of the pixel P_0 is defined as follows:

$$CN(P_0) = \sum_{i=1}^8 (P_i \wedge Q_i) \quad (4)$$

$CN(P_0)$ provides information about the current neighbourhood.

Definition 4. The connectivity number of the pixel P_0 is defined:

$$T(P_0) = \sum_{i=1}^8 c(P_i), \quad (5)$$

where

$$c(P_i) = \begin{cases} 1 & \text{if } ((P_i \wedge Q_i) \wedge (P_{i+1} \wedge Q_{i+1})) \\ 0 & \text{else} \end{cases} \quad (6)$$

$$P_9 = P_1, Q_9 = Q_1$$

The function $T(\cdot)$ is used for the measurement of the connectivity of a pixel in (3×3) -neighbourhood. If it's satisfied $T(P_0) = \min(CN(P_0), 8 - CN(P_0))$, then P_0 is a break point, because it can't be deleted (Zhou et al., 1995). In four cases the P_0 can be deleted without losing the 8th connectivity, these are the following:

Definition 5. The matching function $M(P_0)$ is true, if it corresponds with one of four cases

$$\begin{matrix} 0 & 1 & 0 & 0 & 0 & 0 & 0 & 0 & 0 & 0 & 1 & 0 \\ 0 & 1 & 1 & 0 & 1 & 1 & 1 & 1 & 0 & 1 & 1 & 0 \\ 0 & 0 & 0 & 0 & 1 & 0 & 0 & 1 & 0 & 0 & 0 & 0 \end{matrix} \quad (7)$$

otherwise it is false.

$M(P_0)$ is used for the identification of the break points in P_0 in special cases.

For each pixel P in the Image I , if P is an object pixel, the values $PN(P)$, $CN(P)$, $T(P)$, $M(P)$ are determined by using of the above computations and it is decided whether P may be marked and/or deleted. If no more pixels can be deleted, the skeleton of the object has been received. The modification consists of the fact that we calculate the above values only in the case of the object pixels and we use the following topological condition for marking and deleting of a pixel in the Alg. 1.:

$$PN(P) \neq 8 \wedge [(CN(P) > 1 \wedge CN(P) < 7) \wedge (T(P) = 1 \vee M(P))] \quad (8)$$

Using this modification was achieved a reduced 2×2 line structure on the picture, which means that the skeleton is 1 pixel wide and it can be used easily for the length calculation. It was point out in (Pál, 2003) that the modified Zhou's algorithm is 1 pixel wide, so the skeleton contains 2×2 structures only in some special cases e.g. in the case of few crossing lines etc., but it doesn't contain greater as 2×2 -structures.

The skeletonization algorithm reads as follows:

Algorithm 1 : modified Alg. by Zhou	
FOR $\forall P \in I$	
IF	$P = \text{object pixel}$
THEN	calculate $PN(P), CN(P), T(P)$
IF	$PN(P) \neq 8 \wedge [(CN(P) > 1 \wedge CN(P) < 7) \wedge (T(P) = 1 \vee M(P))]$
THEN	mark pixel
delete the marked pixels	
UNTIL no more pixel can be deleted	

3.4 Fractal Dimension

In numerous investigations for the measurement of biological forms the fractal dimension is used. Accordingly it can be used also for the study of the leaf area. The leaf density is an important characteristic, which can be used for the estimation of the light absorption of the biomass. For the calculation of the leaf density with fractal dimension can be used the panorama picture, the segmented panorama picture and also the 3D data set, where in each pixel of the polar image (R, θ) in place of the intensity the distances of the pixels to the projection plane are used, which is obtained by the formula $d_{pixel} = R * \sin(\theta)$.

The practical computation of the fractal dimension in a binary picture (e.g. Fig. 3 /b/) can carried out via the box dimension or mass radius dimension. The fractal box-dimension is calculated as follows:

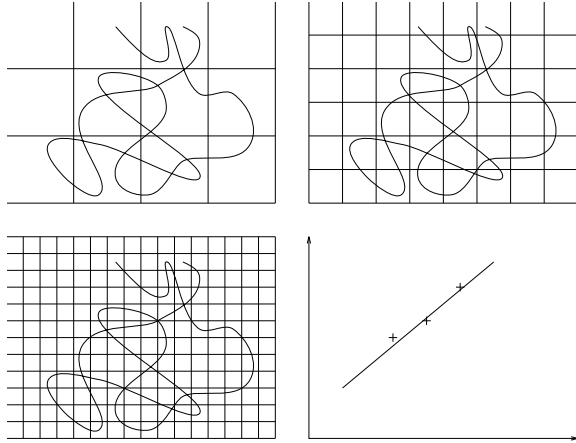


Figure 5: Calculation of the box-dimension

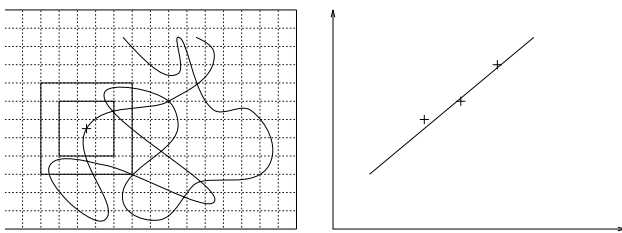


Figure 6: Calculation of the mass-radius-dimension

$$D_B = \lim_{\Delta s \rightarrow 0} \left(-\frac{\log(N(\Delta s))}{\log(\Delta s)} \right) = \lim_{\Delta s \rightarrow 0} \left(\frac{\log(N(\Delta s))}{\log(\frac{1}{\Delta s})} \right). \quad (9)$$

The mass radius dimension D_M can be similarly determined as the box dimension. Here in the binary picture within a square given by its 'radius' (edge length) r the number of object pixels are counted and they are put into the logarithmic coordinate system, where the slope of the fitting straight line is computed (see also Eq. 13), which the mass radius dimension indicates (see Fig. 6).

The box and mass radius dimension can be used also for 3D surfaces, like 'grey value mountains' of the pictures (Chaudhuri and Sarkar, 1992). Here instead of the 2D small boxes 3D cubes are used accordingly, which are determined by the grey values of the picture.

The disadvantage of the above calculations of the fractal dimension is that the pictures must be binarized or segmented. An another method for getting of the fractal dimension is the walking divider method introduced by Shelberg (Turner et al., 1998, p.41). This method uses a chord length (StepLength) and measures the number of chord lengths (NumLength) needed to cover the fractal curve. The technique is based on the principle of taking smaller and smaller rules of size StepLength to cover the curve and computing the number of rules 'NumLength' required in each case. The calculations algorithm of the fractal dimension is based on the following relationship:

$$\text{NumLength} = c \cdot \text{StepLength}^\beta \quad (10)$$

and

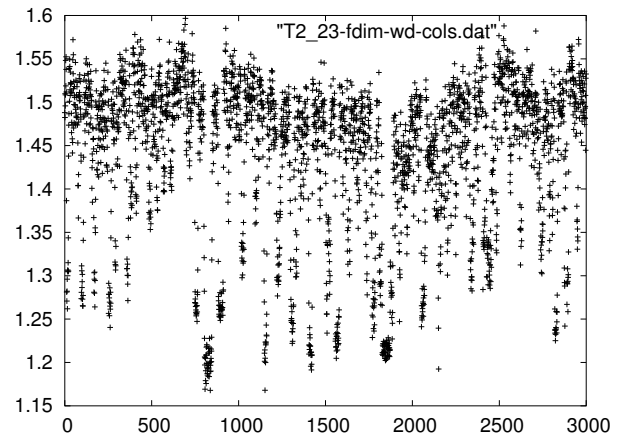
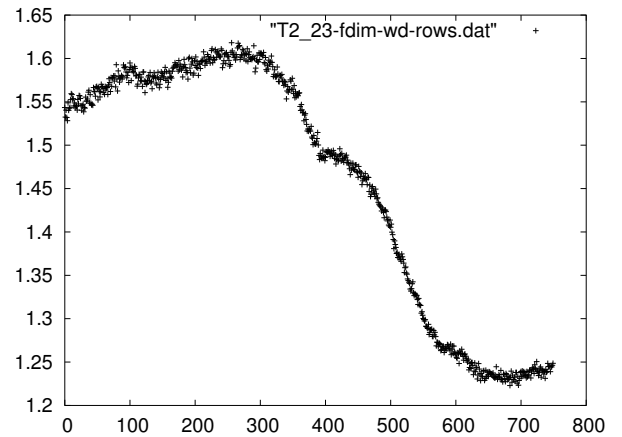


Figure 7: The walking divider fractal dimension (top) on rows and (bottom) on columns calculated on the Fig 3 (a)

$$\log(\text{NumLength}) = \log(c) + \beta \cdot \log(\text{StepLength}). \quad (11)$$

The least squares fit of the bilogarithmic plot of 'NumLength' and 'StepLength' gives the slope β where $D = -\beta$. After differentiating of the error function

$$e = \sum_i (f_i - \beta x_i + c)^2, \quad (12)$$

where f_i corresponds to $\log(\text{NumLength})$ and x_i to the $\log(\text{StepLength})$, with respect to β and c and solving for β we obtain

$$\beta = \frac{N \sum_i f_i x_i - (\sum_i f_i)(\sum_i x_i)}{N \sum_i x_i^2 - (\sum_i x_i)^2}. \quad (13)$$

On the Fig. 7 is shown the fractal dimension using the walking divider method by Shelberg for each row (top) and for each column (bottom). The tree crown and stem structure have higher fractal dimension as the ground area.

4 MEASUREMENTS USING LOCAL DIGITAL GEOMETRY AND TOPOLOGY (LDGT)

Local digital geometry and topology (LDGT) is used for the measurements and extraction of the forest relevant features on the bi-

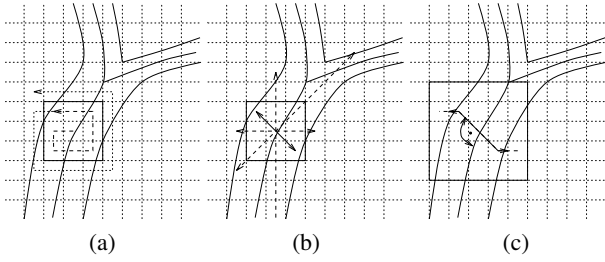


Figure 8: diameter (a) with square filling (b) with directions (c) with orthogonal

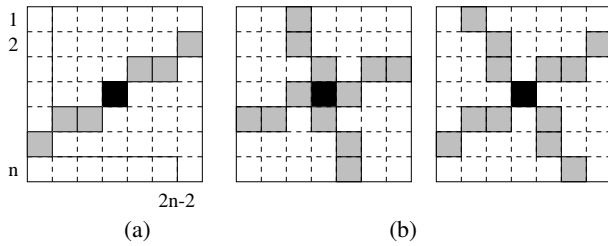


Figure 9: (a) digital line segment in $(n \times n)$ -window, (b) orthogonal digital line segments

nary images, which are obtained after the segmentation and skeletonization of the 2D panorama pictures. For the exact measurement on the 2D images a correction must be applied, to eliminate the perspective distortion and to get a real size of the objects. The perspective correction or the real distance between two pixels on the 2D pictures is calculated from its 3D coordinates using the known vector geometrical formulas.

4.1 Calculation of the Tree Diameter using LDGT

The diameter can be determined in the segmented picture by its different geometrical definition.

A possible procedure for the diameter determination is the square filling out (the algorithm is described in (Pál, 2004)) with the help of the skeleton picture, which is a cover of the tree branches with squares in the tree-emphasized binarized picture (see Fig. 8 /a/). In the skeleton picture can be assigned a value to each pixel of the center line of the tree (similar to (Pál, 2004)), to which the diameter of the cover square corresponds.

To the further algorithms for the tree-trunk diameters calculation the digital line and/or line segment (Klette and Zamperoni, 1995) must be defined (see Fig. 9 /a/).

Definition 6. A digital line segment $L_l^{(n)}$ in a $(n \times n)$ -window $n \geq 3$, $n = 2k+1$, $k \in \mathbb{N}$ is clearly defined by $l \bmod 2(n-1) \in \mathbb{N}$. The pixel coordinates $(dx, dy)^T$ of the digital line segment are to be calculated as follows:

$$\begin{pmatrix} dx(l) \\ dy(l) \end{pmatrix} = \begin{cases} 1, & \text{if } l \in [1, n] \\ l - n - k, & \text{else} \\ 1 + k - l, & \text{if } l \in [1, n] \\ 1, & \text{else} \end{cases}, \quad (14)$$

where $k = \frac{n-1}{2}$.

Another algorithm of the diameter determination is based on the following definition (see also Fig. 8 /b/)

Definition 7. The diameter of a tree-trunk is equal to the minimum distance, which results from the intersections of a digital line segment which lies on a point of the skeleton or a tree-trunk center and the edges of the tree-trunk.

For the determination of the intersection with the edges of the tree-trunk or tree branches two possibilities are offered:

1. The intersection is determined with the help of an edge-segmented picture.
2. The length of the digital line segments is so long increased in both directions, until all pixels of the digital lines are still tree pixels.

With the digital line segment the number of line directions can be determined by the specification of $n \geq 4$.

A further possibility of the diameter determination is based on another geometrical definition of the diameter (see also Fig. 8 /c/)

Definition 8. The diameter of a tree-trunk is the distance, which develops from the intersections of the digital line segment which is perpendicular on its center line and the edges of tree-trunk.

In order to carry out algorithmically the above two definitions of the tree diameters, on the basis of the definition of the digital line segment (Klette and Zamperoni, 1995) a so-called local digital geometry and topology will be mathematically developed. LDGT is based on the representation of the digital line segment by a natural number in a local area given by an $(n \times n)$ -window.

The LDGT can be used not only for the tree-trunk diameter determination, but also for further characteristics of the tree-trunk, like the angle of the branch-bifurcations, the curvature of the tree-trunk and branches etc.

Definition 9. Two digital line segments l_i, l_j in a $(n \times n)$ -windows are together perpendicular ($l_i \perp l_j$) $\Leftrightarrow (l_i + \frac{2(n-1)}{2}) \pmod{2(n-1)} = (l_i + n - 1) \pmod{2(n-1)} = l_j \pmod{2(n-1)}$ thus $l_i + n - 1 \equiv l_j \pmod{2(n-1)}$.

Definition 10. Let $o : \mathbb{N} \rightarrow \mathbb{N}$, $o(l) = (l + n - 1)$ be the perpendicular function or the orthogonal function in a $(n \times n)$ -window.

Theorem 1. $o(\cdot)$ is cyclical mod $2(n-1)$:

$$o(o(l)) \equiv l \pmod{2(n-1)} \quad (15)$$

proof. The proof takes place according to the definition of the orthogonal-function of the digital line segment:

$$\begin{aligned} o(o(l)) &= [l + n - 1] + n - 1 \\ &= l + 2n + 2 \\ &= l + 2(n - 1) \\ l + 2(n - 1) \pmod{2(n - 1)} &= l \pmod{2(n - 1)} \\ o(o(l)) &\equiv l \pmod{2(n - 1)} \end{aligned}$$

□

Definition 11. The bisector l_{wh} from two digital line segments l_i, l_j is the digital line segment

$$l_{wh} \equiv \left\lceil \frac{l_i + l_j}{2} \right\rceil \pmod{2(n-1)}, \quad (16)$$

where $\lceil \cdot \rceil$ means the rounding up.

¹It is naturally considered that the modulo in the interval $[0, n-1]$ and the line segment in the interval $[1, n]$ is. It was neglected only because of the simpler indexation.

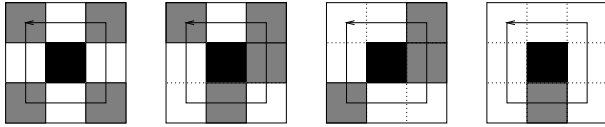


Figure 10: Connectivity number in a (3×3) -window, $C_4^3 = 4$ crossing, $C_4^3 = 3$ bifurcation, $C_4^3 = 2$ normal line and $C_4^3 = 1$ an end pixel structure

Definition 12. A digital curve or straight line area (Pavlidis, 1990) on a discrete lattice are a group of pixels, whose pixels all belong also to the outline of the group, thus in (3×3) -neighbourhood of the pixel no object pixel exists.

For the tree-trunk analysis it is useful to introduce the connectivity number in 4th neighbourhood generally even for larger window $(n > 3)$. The definition for the special case $n = 3$ can be found in (Ernst, 1991).

Definition 13. The connectivity number $C_4^{(n)}$ in a $(n \times n)$ -window is defined:

$$C_4^{(n)} = \frac{1}{2} \sum_{i=1}^{4(n-1)} |P_{i+1} - P_i|, \quad (17)$$

where P_i the border points $(n \times n)$ -window is, thus

$$d_{cs}(P_i(x, y), P_0(x, y)) = \frac{n-1}{2} \quad i = 1, \dots, 4(n-1)$$

and $P_{4(n-1)} = P_1$ (d_{cs} is the Chebychev distance).

The connectivity number is used for the determining about a pixel if it belongs to a crossing $C_4^3 = 4$ or bifurcation $C_4^3 = 3$, to a normal line structure $C_4^3 = 2$ or an end pixel structure $C_4^3 = 1$ (see Fig. 10)

Remark 1. In practice the determination of $C_4^{(n)}$ in the case of greater n by other pixel structures can be disturbed.

Definition 14. Let P_{l_i}, P_{l_j} be the beginning and end points of a digital curve with $C_4^{(n)} = 2$ on the $(n \times n)$ -window border. The perpendicular line segment l_o in the center $(n \times n)$ -window P_0 is defined by the perpendicular of the bisector of the digital line segments of $o(l_i)$ and $o(l_j)$:

$$l_o \equiv o\left(\left[\frac{o(l_i) + o(l_j)}{2}\right]\right) \pmod{2(n-1)} \quad (18)$$

Theorem 2. Let a digital curve be in a $(n \times n)$ -window $C_4^{(n)} = 2$ being connected. Let further be the beginning and end points of the curve P_{l_i}, P_{l_j} on the $(n \times n)$ -window border and accordingly by these points with the center P_0 line segments determined $l_i = (P_{l_i}, P_0), l_j = (P_{l_j}, P_0)$. On the digital curve in P_0 perpendicular digital line segment is through $o\left(\left[\frac{o(l_i) + o(l_j)}{2}\right]\right) \equiv \left[\frac{l_i + l_j}{2}\right] \pmod{2(n-1)}$ given and vice versa.

proof. According to the definition of the perpendicular digital line segment and bisectors with the Thm. 1 follows:

$$\begin{aligned} o\left(\left[\frac{o(l_i) + o(l_j)}{2}\right]\right) &= o\left(\left[\frac{l_i + n - 1 + l_j + n - 1}{2}\right]\right) \\ &= o\left(\left[\frac{l_i + l_j + 2(n-1)}{2}\right]\right) \\ &= o\left(\left[\frac{l_i + l_j}{2}\right] + n - 1\right) \\ &= o\left(o\left(\left[\frac{l_i + l_j}{2}\right]\right)\right) \\ &\equiv \left[\frac{l_i + l_j}{2}\right] \pmod{2(n-1)} \end{aligned}$$

$$\begin{aligned} \left[\frac{l_i + l_j}{2}\right] &= o\left(o\left(\left[\frac{l_i + l_j}{2}\right]\right)\right) \\ &= o\left(\left[\frac{l_i + l_j}{2}\right] + n - 1\right) \\ &= o\left(\left[\frac{l_i + l_j + 2(n-1)}{2}\right]\right) \\ &= o\left(\left[\frac{l_i + n - 1 + l_j + n - 1}{2}\right]\right) \\ &= o\left(\left[\frac{o(l_i) + o(l_j)}{2}\right]\right) \\ &\equiv o\left(\left[\frac{o(l_i) + o(l_j)}{2}\right]\right) \pmod{2(n-1)} \end{aligned} \quad \square$$

With the digital curves it was assumed that they are monotonous between P_{l_i}, P_0 and P_0, P_{l_j} . The monotonously is always attainable, if the size of the window is sufficient small selected.

On the basis of the above mathematical descriptions the tree-trunk diameters can be determined in each skeleton pixel according to the Def. 8. The measurement of the tree-trunk diameters by square filling out is very well suitable for a reconstruction of the tree-trunk from the diameters. The other two procedures (Def. 7, Def. 8) supply against it a more exact diameter, but it can be well determined only outside of the branch bifurcations. On the basis of the diameter the separate representation of the branches and the thicker trunk is possible, as well.

4.2 Extension of the LDGT to 3D

In the above section the 2D LDGT was described, where the 2D digital line segment was represented with a natural number l . In 3D space will be needed two natural numbers $(l, k), l, k \in \mathbb{N}$ to represent a 3D digital line segment. The first number is used for the orientation in the horizontal space and the second number in the vertical space. A similar extension is used also for the skeletonization. The calculation of the intersection of the orthogonal of a 3D digital curve to the object surface is more complicated and computationally intensive process, because of the surface modeling.

4.3 Circle/ellipse detecting and fitting

The detecting of circles and ellipses such as the tree-trunk slice in the 3D scene e.g with Hough transformation is a very time-consuming task (searching in the 3-5 dimensional space). Using the LDGT on the 2D panorama pictures with the help of the 3D-coordinates it is possible to reduce the circle/ellipse detection time. On the segmented 2D panorama pictures and with the help of LDGT and of the 3D geometry the 3D points near to an orthogonal plane in a tree trunk position can be extracted, which 378 points belong to the stem boundary. After the projection of these

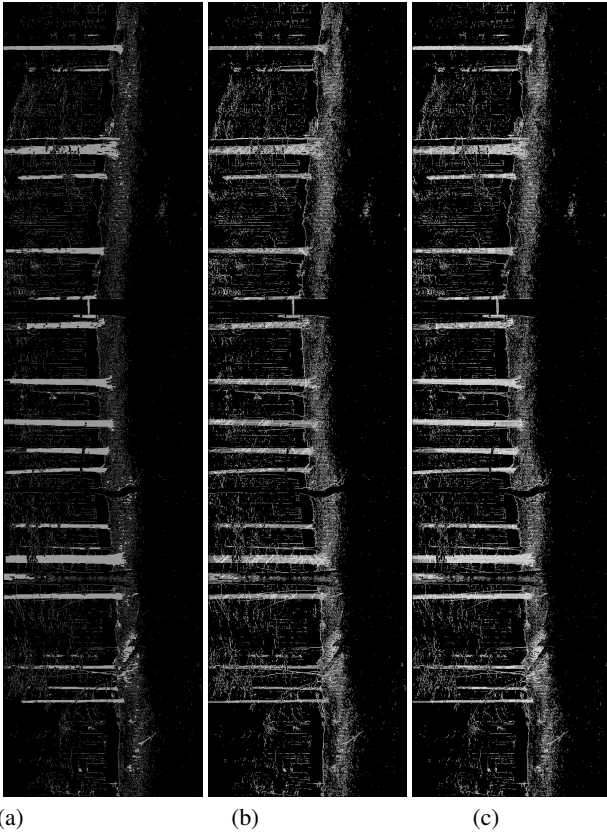


Figure 11: The pictures are 90 degree rotated. The reconstruction of the tree structures from the tree diameters in the skeleton pixels (a) with square filling, (b) with minimal length and (c) with orthogonals

points to the orthogonal plane to the tree-trunk can be used any regression approach to determinate the stem border and the stem diameter at this position.

For the circle/ellipse fitting the algebraic equation was used:

$$F(x, y) = Ax^2 + Bxy + Cy^2 + Dx + Ey + F \quad (19)$$

which in th case of the circle is:

$$F(x, y) = x^2 + y^2 + Dx + Ey + F \quad (20)$$

and the least squares method with the error function

$$e = F(x, y; D, E, F)^2. \quad (21)$$

The $D, E,$ and F minimize e if the partial derivatives for e with respect to each of $D, E,$ and F are simultaneously zero (Eq. 24). To determinate the center point (xc, yc) and the radius r of the circle must be solved the Eq. 25 and

$$xc = -D, yc = -E \quad (22)$$

and

$$r = \sqrt{xc * xc + yc * yc - F}. \quad (23)_{379}$$

$$\begin{aligned} \frac{\partial e}{\partial D} &= \sum_i 2(x_i^2 + y_i^2 + Dx_i + Ey_i + F) \cdot x_i \\ &= \sum_i 2(x_i^3 + y_i^2 x_i + Dx_i^2 + Ey_i x_i + Fx_i) = 0 \\ \frac{\partial e}{\partial E} &= \sum_i 2(x_i^2 + y_i^2 + Dx_i + Ey_i + F) \cdot y_i \\ &= \sum_i 2(x_i^2 y_i + y_i^3 + Dx_i y_i + Ey_i^2 + Fy_i) = 0 \\ \frac{\partial e}{\partial F} &= \sum_i 2(x_i^2 + y_i^2 + Dx_i + Ey_i + F) \\ &= \sum_i 2(x_i^2 + y_i^2 + Dx_i + Ey_i) = 0 \end{aligned} \quad (24)$$

$$\begin{aligned} 2 \sum_i x_i^2 D + 2 \sum_i x_i y_i E + \sum_i x_i F + \sum_i x_i^3 + x_i y_i^2 &= 0 \\ 2 \sum_i x_i y_i D + 2 \sum_i y_i^2 E + \sum_i y_i F + \sum_i y_i^3 + x_i^2 y_i &= 0 \\ 2 \sum_i x_i D + 2 \sum_i y_i E + \sum_i 1 F + \sum_i x_i^2 + y_i^2 &= 0 \end{aligned} \quad (25)$$

The ellipse fitting is analogous to the circle least squares method. Here is used the Eq. 19 and also the parameters A, B, C should be determinated.

The approximation of the extracted 3D-points is possible by using splines, principal curves or another methods, as well.

5 RESULTS AND DISCUSSION

Using LDGT with the help of the connectivity numbers can be followed the skeleton-pixels with $C_4^3 >= 2$ in each column from the beginning on the ground area (the 1st skeleton-pixel with $C_4^3 = 1, = 3$ or $= 4$) to the tree-top or the highest possible part of the tree on the picture (the last skeleton-pixel with $C_4^3 = 1, = 3$ or $= 4$). Small skeleton-parts can be assumed as noisy and excluded from the calculations, so only the representative skeleton-parts are used. The real (x,y,z) -coordinates of the beginning and of the end-pixels of the tree-skeleton give the tree height. If the tree-skeleton is broken it results of course a wrong tree height. Walking on the tree-skeleton at approx. 1,3m height from the beginning pixel, the pixels are cutted with the help of one of the suggested diameter-algorithms and the corresponding 3D-coordinates are used for tree-trunk diameter calculation. The DBH can be determinated e.g. using circle/ellipse fitting (see Sec. 4.3). Following again the skeleton pixels on the skeleton curve the connectivity numbers help to find the branches on the tree or the skeleton line. The third skeleton pixel with $C_4^3 = 4,$ or $C_4^3 = 3$ should be mean the beginning of the crown according to the forestry definitions ('at the 3rd green branches'), but in our case currently it isn't possible to determinate the colour of the branches. Another problem is, if the branch cannot or can be only particularly seen on the scan.

Although the above algorithms are able to measure the exact sizes, the noise (e.g. which may result broken or extra skeleton parts) or the situation that one-scan contains not always the whole information about the complete tree, must be kept in mind.

The suggested algorithms make possible the automatical extraction and calculation of the relevant forest parameters on the whole data set, but not only in one measured point (e.g. in the case of the DBH, which is used mostly in the forestry), but at every user defined heights. So for example also the stem form (also curvature/torsion of the stem) can better calculated, which was so far only on the harvested tree possible. In the case of more scans from an inventory point from different scan positions the one-scan algorithms can complete the algorithms which were developed for the merged 3D data set. This algorithms can be used as well in the one-scan case, but in view of the fact that the data set may contain not enough information for the correct measurements. For example, we assume that the 3D-coordinates of a

tree are extracted with manual or region of interest (ROI) based technique, or automatically, where the trees, tree-foot positions can be localized by the local maxima in the distance-histogram, which contains the occurrence of the object-points with the same distance-ranges to the camera plane in a pixel-column in the case of the panorama pictures or in a given grid structure in the case of the merged 3D data set. A small fraction of the lowest (z-coordinate) points are used for the determination of the local tree foot-position, which is calculated by the mean of the x,y-coordinates of these points. From the tree foot position in 1,3m height the pixels are cutted and used for the DBH calculation with the circle fitting method. The crown base is determined by the mean radial distances at each height by given step size. If the mean radial distance and its standard deviation are significantly different from the values at DBH, then the crown base is at this height. For the crown can be derivated the same sizes such the mean radii and the crown dimensions can be calculated. The tree height is the difference between the z-coordinates of the tree foot-position and the mean of a small percentage of the highest points.

6 CONCLUSIONS AND FUTURE WORK

In this work there were suggested algorithms and mathematical founded methods for the segmentation, skeletonization and digital measurements using LDGT. The purposed algorithms support the manual, ROI based measurements and make possible the automatical and computer based measurements on digital pictures and terrestrial laser data. The extraction of forest relevant parameters are based on the using of pictures as digital masks (segmented and skeletonized pictures) and on calculating the distances, lengths along the line structures and n-connected digital pixel structures (digital curves) in a local area which are determined by LDGT.

The tree segmentations method works well if the intensity information from the tree (bright) is quite different from the background information (black). There are some trees see also on the Fig. 3 (a) where the tree trunk is so dark as the background. In this case the range information should be used to distinguish it from the background. The quality of the segmentation influences mainly the skeletonization and also the digital measurements using LDGT. In the ideal case the exact object sizes can be determined, but the intensity values of the laser data are not always enough to detect all tree structures. Because of it the segmentation on 2D panorama pictures should be extended for the 3D data set to get better preprocessing result. The colour information and its projection to the 3D data set are also necessary to separate the crown and leaf structures from the tree stem and branches and from the ground area.

We have seen that only the intensity picture is not enough for the real size measurements, but it supports very well the extraction of the forest inventory parameters in the case of the above techniques. There are methods like the fractal dimension which can be used independent from the segmentation also for the 3D data set and it makes the characterization of the different forest structures, biomass etc. possible (see Fig. 7 /top/). Furthermore the fractal dimension can be used without size or range and distance information also only on the intensity or panorama picture.

ACKNOWLEDGEMENTS

The Authors would like to express their gratitude to the project partners from the Forest Management Institute (FMI /ÚHÚL/) Brandýs nad Labem, in Czech Republic, and to the Bavarian Ministry INTERREG III A which supplies funding for the project. 380

REFERENCES

- Bräunl, T., Feyer, S., Rapf, W. and Reinhardt, M., 1995. *Parallele Bildverarbeitung*. Addison-Wesley (Deutschland) GmbH, Bonn.
- Chaudhuri, B. B. and Sarkar, N., 1992. An efficient approach to compute fractal dimension in texture image. In: *Computer Vision and Applications, Proceedings of the 11th Int. Conf. on Pattern Recognition*, Vol. 1., International Association for Pattern Recognition(IAPR), IEEE Computer Society Press, Hague, Netherland, pp. 358-361.
- Datta, A. and Parui, S. K., 1994. Performs a thinning of a binary input image. *Pattern Recognition* 27(9), pp. 1181-1192.
- Dyer Charles, R. and Rosenfeld, A., 1979. Thinning algorithms for gray-scale pictures. *IEEE Trans. on Pattern Analysis and Machine Intelligence* 1(1), pp. 88-89.
- Ernst, H., 1991. *Einführung in die digitale Bildverarbeitung: Grundlagen und industrieller Einsatz mit zahlreichen Beispielen*. Franzis-Verlag GmbH, München.
- Ge, Y. and Fitzpatrick, J. M., 1996. On the generation of skeletons from discrete euclidean distance maps. *IEEE Trans. on Pattern Analysis and Machine Intelligence* 18(11), pp. 1055-1066.
- Klette, R. and Zamperoni, P., 1995. *Handbuch der Operatoren für die Bildbearbeitung*. 2. üb. edn, Vieweg Verlag, Braunschweig.
- Pavlidis, T., 1990. *Algorithmen zur Graphik und Bildverarbeitung*. Heinz Heise Verlag, Hannover.
- Pál, I., 2002. Ein Vergleich der Gefäßsegmentierungsverfahren auf SLDF-Perfusionsbildern. In: M. Meiler, D. Saupe, F. Kruggel, H. Handels and T. Lehmann (eds), *Bildverarbeitung für die Medizin 2002: Algorithmen-Systeme-Anwendungen Proceedings des Workshops in Leipzig*, Informatik aktuell, Springer-Verlag, Berlin, pp. 378-381.
- Pál, I., 2003. Ein Skelettierungsalgorithmus für die Berechnung der Gefäßlänge. In: T. Wittenberg, P. Hastreiter, U. Hoppe, H. Handels, A. Horsch and H.-P.Meinzer (eds), *Bildverarbeitung für die Medizin 2003: Algorithmen-Systeme-Anwendungen Proceedings des Workshops in Leipzig*, Informatik aktuell, Springer-Verlag, Berlin, pp. 71-75.
- Pál, I., 2004. Zeitbedarf des Algorithmus für die Berechnung des gefäßfreien Gebietes. In: *Bildverarbeitung für die Medizin 2004: Algorithmen-Systeme-Anwendungen Proceedings des Workshops in Leipzig*, Informatik aktuell, Springer-Verlag, Berlin, pp. 115-119.
- Pál, I. and et al., 1996. Erkennung von Mikrozirkulationsstörungen der Netzhaut mittels "Scanning Laser Doppler Flowmetrie". In: T. Lehmann, I. Scholl and K. Spitzer (eds), *Bildverarbeitung für die Medizin: Algorithmen-Systeme-Anwendungen Proceedings des Aachener Workshops*, Verlag der Augustinus Buchh., Aachen, pp. 89-94.
- Riazanoff, S., Cervelle, B. and Chorowicz, J., 1990. Parametrisable skeletonization of binary and multilevel images. *Pattern Recognition Letters* 11, pp. 25-33.
- Sirjani, A. and Cross, G. R., 1991. On representation of a shape's skeleton. *Pattern Recognition Letters* 12, pp. 149-154.
- Turner, M. J., Blackledge, J. M. and Andrews, P. R., 1998. *Fractal Geometry in Digital Imaging*. Academic Press, San Diego, California.
- Zamperoni, P., 1989. *Methoden der digitalen Bildsignalverarbeitung*. Vieweg Verlag, Braunschweig.
- Zhou, R. W., Quek, C. and Ng, G. S., 1995. A novel single-pass thinning algorithm and an effective set of performance criteria. *Pattern Recognition Letters* 16, pp. 1267-1275.